Understanding the emplacement of Martian volcanic rocks using petrofabrics of the nakhlite meteorites.

Luke Daly[1,5,6*], Sandra Piazolo[2], Martin R. Lee[1], Sammy Griffin[1], Peter Chung[1], Fabrizio Campanale[1], Benjamin E. Cohen[1], Lydia J. Hallis[1], Patrick W. Trimby[3], Raphael Baumgartner[4], Lucy V. Forman[5], Gretchen K. Benedix[5,7]

[1]School of Geographical and Earth Sciences, University of Glasgow, Glasgow, G12 8QQ, UK.

[2]School of Earth and Environment, University of Leeds, Leeds, LS2 9JT, UK

[3]Oxford Instruments Nanoanalysis, High Wycombe, HP12 3SE, UK

[4]School of Biological, Earth and Environmental Sciences, The University of New South Wales, Kensington, NSW, 2052, Australia.

[5]Space Science and Technology Centre, School of Earth and Planetary Sciences, Curtin University, GPO Box U1987, Perth, WA 6845, Australia.

[6]Australian Centre for Microscopy and Microanalysis, University of Sydney, Sydney 2006, NSW, Australia.

[7]Planetary Science Institute, 1700 East Fort Lowell, Suite 106 Tuscon, AZ, 85719-2395 USA

*luke.daly@glasgow.ac.uk

Abstract

In order to validate calculated ages of the Martian crust we require precise radiometric dates from igneous rocks where their provenance on the Martian surface is known. Martian meteorites have been dated precisely, but the launch sites are currently unknown. Inferring the formation environment of a correlated suite of Martian meteorites can constrain the nature

and complexity of the volcanic system they formed from. The nakhlite meteorites are such a suite of augite-rich rocks that sample the basaltic crust of Mars, and as such can provide unique insights into its volcanic processes. Using electron backscatter diffraction we have determined the shape-preferred and crystallographic-preferred orientation petrofabrics of four nakhlites (Governador Valadares, Lafayette, Miller Range 03346 and Nakhla) in order to understand the conditions under which their parent rocks formed. In all samples, there is a clear link between the shape-preferred orientation (SPO) and crystallographic-preferred orientation (CPO) of augite phenocrysts. This relationship reveals the three-dimensional shape of the augite crystals using CPO as a proxy for SPO, and also enables a quantitative 3-dimensional petrofabric analysis. All four nakhlites exhibit a foliation defined by the CPO of the augite <c> axis in a plane, although individual meteorites show subtle textural variations. Nakhla and Governador Valadares display a weak CPO lineation within their <c> axis foliation that is interpreted to have developed in a combined pure shear/simple shear flow regime, indicative of emplacement of their parent rock as a subaerial hyperbolic lava flow. By contrast, the foliation dominated CPO petrofabrics of Lafayette and Miller Range 03346 suggest formation in a pure shear dominated regime with little influence of hyperbolic flow. These CPO petrofabrics are indicative of crystal settling in the stagnant portion of cooling magma bodies, or the flattening area of spreading lava flows. The CPO foliation of Lafayette's is substantially weaker than Miller Range 03346, probably due to its higher phenocryst density causing grain-grain interactions that hindered fabric development. The CPO petrofabrics identified can also be used to determine the approximate plane of the Martian surface and the line of magma flow to within ~20°. Our results suggest that the nakhlite launch crater sampled a complex volcanic edifice that was supplied by at least three distinct magmatic systems limiting the possible locations these rocks could have originated from on Mars.

Keywords: Mars, Martian meteorites, nakhlites, electron backscatter diffraction, petrofabrics, magmatic petrogenesis.

1. Introduction

The petrogenetic study of Martian meteorites and their inferred geological environment can help us constrain the specific site these rocks were launched from on the planet's surface. Ultimately, this knowledge will provide ground truth for crater counting calculations of the age of Mars' crust. In addition, the study of Martian igneous rocks provides insights into volcanism on a planetary surface with stagnant lid tectonics. The nakhlite meteorites are a suite of pyroxene-rich (predominantly augite; ~65-80 modal %) mafic igneous rocks from Mars (Bogard & Johnson, 1983; Treiman, 2005; Corrigan *et al.*, 2015). They are comprised of elongate, subhedral to euhedral prisms of augite, rarer olivine phenocrysts, and varying abundances of interstitial fine-grained mesostasis (Treiman, 2005). These meteorites also contain minerals including phyllosilicates and carbonates that formed by post-magmatic aqueous alteration (Ashworth & Hutchison, 1975; Bunch & Reid, 1975; Changela & Bridges, 2010; Hallis *et al.*, 2012, Hicks *et al.*, 2014; Bridges *et al.*, 2019). The nakhlites have been relatively mildly shocked (<15 GPa; Treiman, 2005) interpreted to be a result of impact-ejection from the Martian surface in a single event (Treiman, 2005).

The petrogenesis of the nakhlites has conventionally been interpreted as either a single intrusion or a thick lava flow (Harvey & McSween, 1992; Nyquist *et al.*, 2001; Mikouchi *et al.*, 2003; Treiman, 2005; Day *et al.*, 2006; Mikouchi *et al.*, 2012; Richter *et al.*, 2016). A potential terrestrial analogue is Theo's flow (Ontario, Canada; Lentz *et al.*, 1999). However, their formation in a single magmatic event has recently been challenged by $^{40}Ar/^{39}Ar$

crystallization ages requiring at least four episodes of igneous activity within the nakhlite meteorite suite over a timespan of ~91 Ma (i.e. 1416 ± 7 Ma to 1322 ± 10 Ma; Cohen *et al.*, 2017).

In this study we assess whether petrofabrics can be used to understand the conditions under which the nakhlites formed, and so help to discriminate between the different models for their emplacement (e.g. single vs multiple igneous bodies). Using hand specimen and transmitted light petrography, shape-preferred orientations (SPOs) of elongate augite phenocrysts have been reported for the meteorites Nakhla, Lafayette and Yamato (Y) 000593 (Bunch & Reid, 1975; Mikouchi *et al.*, 2003). Berkley *et al.* (1980) described a foliation and lineation in Governador Valadares, Nakhla and Lafayette, formed by the preferred orientation of the long <c> axes of augite crystals. In contrast, recent studies that have used image processing to describe crystal shapes and to determine the crystal size distributions have concluded that the nakhlites lack a petrofabric (Lentz *et al.*, 1999; Udry & Day, 2018). Lentz *et al.* (1999) also concluded that the crystal size distribution of augite phenocrysts in nakhlites is characteristic of steady state nucleation and continuous growth. However, these previous studies have been limited by the difficulties inherent in relating 2D measurements of grain size and shape in thin section to 3D shape and crystallographic orientations.

Different styles of emplacement of igneous rocks generate distinctive petrofabrics that can be identified and quantified using 3D crystallographic information. For example, phenocryst-bearing terrestrial lavas display a weak to moderately strong lineation in the long shape axis of phenocrysts due to shear forces aligning long axes to the flow direction (Bhattacharyya, 1966). In some instances, a short shape axis lineation oriented perpendicular to the direction of flow is also observed (Bascou *et al.*, 2005; Boiron *et al.*, 2013). Conversely, magmatic

fabrics derived from gravity settling in an intrusion or stagnant lava pond produce a short shape axis lineation parallel to the gravitational force, as well as an associated, planar girdle distribution in the long axis perpendicular to the gravitational force (e.g., Jackson, 1961; George, 1978). Hence, crystal shape fabrics in terrestrial lavas have been used as kinematic indicators to reconstruct their flow history (e.g., Shelley, 1985; Wada, 1992; Ventura *et al.*, 1996). In addition, numerical models predict that the development of a petrofabric is typically dependent on the flow regime, where a combined lineation and foliation of the long shape axes of crystals is predicted to form in a regime resulting from an oblate strain. Such strain can occur in a so called "hyperbolic" flow characterized by a combination of simple and pure shear flow (e.g. Merle, 1998; Iezzi & Ventura, 2002).

Unconstrained growth of a mineral grain in a fluid, such as molten rock, typically produces a strong correlation between the shape of a crystal and its crystallographic orientation (e.g., the crystal's <c> axis being parallel to the long shape axis of the crystal; Benn & Allard, 1989). These fabrics, such as 2D-SPO and crystallographic-preferred orientation (CPO), can be quantitatively described through electron backscatter diffraction (EBSD) mapping (Prior *et al.*, 1999). Therefore, EBSD is a suitable tool for quantitatively investigating the petrofabrics of the nakhlite meteorites and constraining the mechanisms of their magmatic emplacement. Here we have used EBSD mapping to investigate the conditions under which Miller Range (MIL) 03346, Lafayette, Governador Valadares and Nakhla formed. These meteorites are of particular interest because they differ significantly in mineralogy, including the abundance of olivine (Lafayette > Nakhla = Governador Valadares > MIL 03346) and mesostasis (MIL 03346 > Lafayette = Governador Valadares > Nakhla; Corrigan *et al.*, 2015; Udry & Day, 2018), and also differ in the crystallinity of the mesostasis and thickness of reaction rims on olivine and pyroxene (Treiman 2005; Mikouchi *et al.*, 2003).

2. Methods

Thin sections of the nakhlite meteorites MIL 03346 (118), Lafayette (USNM 1505-5), Governador Valadares (Natural History Museum, London) and Nakhla (WAM 12965) were obtained on loan from museum collections. As such, they were not specifically cut relative to the orientation of any fabrics in these meteorites such as lineations or foliations. These sections were prepared for EBSD analysis by progressively mechanically polishing each sample from 8 µm grit paper (five minutes) to 1 µm and 0.3 µm suspension of aluminium balls in glycol (five minutes each). They were then polished further in a NaOH colloidal silica (0.1µm) suspension for four hours to remove the damaged layer from the initial mechanical polish so as to provide a surface suitable for EBSD. Governador Valadares and Nakhla were coated with 5 nm of carbon for high vacuum EBSD work at Macquarie University, while MIL 03346 and Lafayette were not coated, in order to take advantage of the variable pressure scanning electron microscope (VP-SEM) at the University of Glasgow.

SEM secondary electron imaging, as well as energy dispersive X-ray spectroscopy (EDS) and EBSD data analysis of MIL 03346 and Lafayette used a Zeiss Sigma VP field emission gun SEM (VP-FEGSEM) operated at a vacuum of 49 Pa, at the University of Glasgow. This instrument is equipped with an Oxford Instruments X-Max 80 mm^2 silicon drift X-ray detector and a NordlysMax^2 EBSD detector.

SEM, EDS and EBSD data were acquired for Nakhla and Governador Valadares using a Carl Zeiss IVO SEM operated at high vacuum, at Macquarie University. This instrument is equipped with a HKL NordlysNano high sensitivity EBSD detector.

In both SEM laboratories, EBSD data were acquired with and indexed using Oxford Instruments' AZtec software. For all EBSD analyses, the samples were tilted to 70 °, the standard angle used for EBSD, and data were collected at 20 kV/4-8 nA via the automated Large Area Mapping module of AZtec 3.3. The rectangular areas analysed by EBSD were: 106.4 mm^2 at a step size of 4 µm for MIL 03346; 85.0 mm^2 at a step size of 4 µm for Lafayette; 20.3 mm^2 at a step size of 15 µm for Governador Valadares; 13.3 mm^2 at a step size of 15 µm for Nakhla. These analyses produced combined totals of 6.6 million, 5.3 million, 0.09 million and 0.06 million electron backscatter patterns (EBSP) for MIL 03346, Lafayette, Governador Valadares, and Nakhla, respectively. The expected angular uncertainty for each individual EBSD measurement is <0.5° (Borthwick and Piazolo, 2010). In order to facilitate rapid whole section mapping, EBSPs were analysed in Oxford Instruments AZtec 3.3 software using 4×4 binning, an exposure time of 30-40 ms, and a frame average of 1 frame. The mean angular deviation (MAD), which is an expression of the quality of pattern indexing (<1 is considered appropriate), was 0.52-0.61 for augite in all samples. The data were cleaned using Oxford Instruments HKL software Channel 5, involving a wildspike correction to remove isolated data points, followed by an iterative 8-, and 7-point nearest neighbour zero solution and a single 6-point nearest neighbour zero solution. This procedure helps to define grains without creating artefacts (i.e. Bestmann & Prior, 2003; Watt *et al.*, 2006). As the thin sections being studied were prepared without reference to any rock fabric, we define a reference frame where x = horizontal, y = vertical, and z = perpendicular (out of the plane of the thin section), and which relates directly to the x, y, z orientation of the rectangular analysis area chosen for EBSD maps. This reference frame is consistent for each sample between maps, pole figures, and rose diagrams presented.

Grain boundaries within the datasets were defined by <10 ° misorientation across adjacent pixels. To avoid grain statistical artefacts related to minute mesostasis grains and fractured phenocrysts, only the grains larger than 100 µm in circle equivalent diameter were used for further analysis. We define a grain as an area that is fully enclosed by grain boundaries. Twin boundaries in augite, which are defined by a 180 ° rotation around (100), (001), (204) or (104), were disregarded so that twinned grains were not sampled multiple times. Crystallographic and shape orientation data were extracted from a statistically significant number of augite grains in each sample. More than 100 grains are required to define a representative fabric in a given rock (e.g., Ismaıl & Mainprice, 1998; Watt *et al.*, 2006) and we analysed 1382 augite grains in MIL 03346, 2225 in Lafayette, 390 in Governador Valadares, and 329 in Nakhla. To display any CPOs in the augite phenocryst population, one representative crystallographic orientation was extracted per grain.

CPOs for the augite phenocrysts are assessed with reference to their three major crystallographic axes (<a> = <100>, <b> = <010>, <c> = <001>). The poles to these axes are plotted in a lower hemisphere, stereographic projection (pole figure), and the data are contoured relative to the density of data points, expressed as multiples of uniform density (m.u.d.).

In order to determine the strength of the CPO, two quantitative metrics were calculated: M-index (Skemer *et al.*, 2005) and J-index (Bunge, 2013). The M-index defines the variance in uncorrelated misorientation angle distributions between the sample crystallographic data and a theoretical random fabric by taking all major (low index) axes into account (e.g., for augite <100>, <101> and <001>). An M-index of 0 represents a random crystallographic orientation distribution while 1 denotes a single crystal. In contrast, the J-index (or texture index) is

defined as the volume-averaged integral of squared orientation density of a chosen axis (here <001> was used). J-index values range from 1, representing a random crystallographic orientation distribution, to infinity, which is a single crystal. For all nakhlites in this study, the M-index and J-index were calculated using the MTEX toolbox for MATLAB with a kernel halfwidth of 10 (Bachmann *et al.*, 2010). Finally, we performed eigenvalue analysis to quantify the dominant, crystallographic fabric type, distinguishing between point (P), girdle (G), and random (R) fabric (Vollmer, 1990). This analysis (PGR) demonstrates whether a specific axis forms a lineation (perfect alignment forming a "Point" fabric), a foliation (alignment of grains in one plane forming a "Girdle" fabric), or none of the above ("Random" fabric). For each major crystallographic axis, the contribution of P, G, or R can be calculated from three normalized eigenvalues $(k_1 k_2 k_3)$: $P = k_1 - k_3$, $G = 2(k_2 - k_3)$, and $R = 3k_3$. The MATLAB-MTEX code for these calculations is provided in the supplementary materials. Due to the nature of geological materials, pure 100% P or G endmembers are uncommon; even rocks with strong foliations or lineations are unlikely to exhibit P or G values much above 50%. Therefore, here we infer a random fabric only when $R > 90$ %. P or G values between 10-30 % are interpreted as weak fabrics, while 30-50% denote moderate fabrics and >50% represent a strong fabric.

3. Results

3.1. Morphology of augite phenocrysts

It is clear that grain boundaries are commonly formed by low index planes (i.e. facets) in the EBSD data; hence grains represent phenocrysts. The augite phenocrysts are subhedral to euhedral and exhibit an elongate shape parallel to their <c> crystal axis as evidenced in crystals where the <c> axis is parallel to the plane of the thin section (Figure 1). The two short shape axes correlate with the <a> and <b> crystal axes as evidenced in crystals where

the <a> and <b> crystal axes are parallel to the plane of the thin section. Thus, the augite phenocrysts are prism-shaped, not tabular (Figure 1).

3.2. SPO and CPO

The long shape axes of augite phenocrysts in Nakhla and Governador Valadares lack a strong 2D-SPO, as evidenced by their rose diagrams lacking a distinct clustering of long shape axis orientations (Figures 2B, 3B). By contrast, Lafayette and MIL 03346 have a clear 2D-SPO as evidenced by the clustering of long shape axes in their rose diagrams (Figures 4, 5). Lafayette is characterised by a relatively narrow spread of 2D-SPO (~40°), while MIL 03346 has a wider spread (~80°) (Figures 4, 5).

CPO patterns differ between the four meteorites. Pole figure m.u.d. values for Nakhla, MIL 03346 and Governador Valadares highlight weak <a> crystal axis point maxima perpendicular to a moderate <c> crystal axis girdle (Figures 2-4). Within the <c> crystal axis girdle plane of Nakhla, MIL 03346 and Governador Valadares, clustering of higher m.u.d. values in the pole figure reveals weak point maxima (Figures 2C, 3C, 5C). Lafayette pole figure m.u.d. values show that its augite grains define a weak <c> crystal axis girdle (Figure 4C). There is a clear correlation between the 2D-SPO long axis and <c> axis CPO orientation for MIL 03346 (Figure 5), which is consistent with our observations in Figure 1 that grain shapes are crystallographically controlled (i.e., the <c> axis of augite correlates with long crystal shape axis) and permits us to infer 3D-SPO information from the CPO data.

Quantitative textural metrics for the meteorites support the qualitative textural observations from the contoured m.u.d. values in EBSD pole figures. The four nakhlites have J-indices of 2-3, which indicates a moderate <c> axis CPO (Figure 2-5). PGR metrics indicate that all

samples have a moderate girdle fabric in the <c>/(001) crystal axis (Figure 6), although this fabric is weaker in Lafayette than in the other three nakhlites (Figure 6). In addition, Nakhla and Governador Valadares exhibit a weak <c> crystal axis point fabric (Figure 6). This point fabric is also apparent as high m.u.d. values contained within the girdle of the <c> crystal axis pole figure (Figure 2C and 3C). With regards to the other crystallographic axes, there is a weak (100) CPO point fabric in Nakhla, MIL 03346 and Governador Valadares. However, in all four nakhlites the M-index is uniformly low (0.01-0.03) (Figure 2-5).

4. Discussion

We first appraise the potential of our sample set for describing petrofabrics in 3D, then evaluate how the properties of magma can be inferred from the petrofabric of rocks that have formed after its solidification. Based on this understanding we then discuss the magmatic conditions under which the four nakhlites formed, and the implications of our findings for the petrogenesis of the nakhlite suite as a whole.

4.1. Inferring 3D fabrics from 2D data: limitations and implications

For samples of modern terrestrial lava flows, their original orientation relative to the Earth's surface, proximity to the original magmatic system, and flow direction are all known. This crucial contextual information has been lost from the nakhlites as these meteorites were impact ejected from Mars into space. In addition, at a hand specimen scale it is difficult to unambiguously identify any fabrics, such as foliations or lineations. Therefore, the nakhlite thin sections studied here, which are essentially 2D slices through these meteorites, would not have been cut with respect to any visible rock fabrics so that any 2D-SPO identified may not correspond to the maximum 3D-SPO. Thus, the absence of a 2D-SPO in the Nakhla and Governador Valadares thin sections does not necessarily preclude its presence in these

meteorites. Fortunately, the shape of augite phenocrysts in the nakhlites is crystallographically controlled, whereby the crystal c-axis is parallel to the long shape axis of the crystal and the crystal b- and a- axes form the short shape axes (Figure 1). Thus, the drawback of having a randomly selected 2D plane of observation inhibiting the characterisation of a 3D-SPO can be overcome by using quantitative crystallographic orientation of all axes derived from EBSD as a proxy for the full 3D-SPO of phenocrysts. The following discussion therefore emphases CPO rather than 2D-SPO, as the CPO is independent of the cut of the thin section.

4.2. The relationship between CPO fabrics and magmatic flow regimes

Igneous rocks that contain phenocrysts with shape anisotropy (e.g., prismatic or tabular) in a finely crystalline groundmass, usually exhibit distinct 3D-SPO and CPO fabrics that are characteristic of specific magmatic regimes. These fabrics can be identified using EBSD where crystal shape is crystallographically controlled (i.e., the long and short shape axes correspond to crystallographic planes) (Figure 1). Three end-member fabrics can be identified:

(1) Random crystallographic orientation. This fabric would lack clustering or distinct patterns of crystal orientation (i.e., no preferred alignment of elongate phenocrysts). The absence of CPO indicates a mode of emplacement whereby no consistent directional force has been applied to the cooling phenocryst-matrix assemblage. Such magmatic environments include both turbulent flow and flow characterized by instabilities, such as convection cells. Other scenarios that would produce a random crystallographic orientation include: (i) a 2D simple shear flow, where orientations fluctuate significantly and can cyclically reach minimum values; (ii) high phenocrysts to matrix ratios that inhibit phenocryst rotation and so fabric

development (Ježek *et al.*, 1996). This fabric is not observed in any of the nakhlites studied here.

(2) A CPO that is characterised by one or two crystal axes lying in a plane is called a magmatic foliation (Paterson *et al.*, 1998). Pole figures with such a CPO show a girdle distribution of the long axis of prism shaped phenocrysts, and two girdles of the two longest axes of tabular phenocrysts. This type of CPO indicates a deformation regime dominated by pure shear or flattening flow with $\sigma1>\sigma2=\sigma3$. Such a pure shear regime occurs during gravitational crystal settling and compaction in quiescent areas of stagnant magmatic bodies, such as lava pools and ponds, or magmatic intrusions (Merle, 1998; Iezzi & Ventura, 2002). All nakhlites exhibit this fabric, but it is dominant in Lafayette and MIL 03346 (Figure 2, 3, 4, 5).

(3) A CPO featuring a distinct alignment of the long axes of tabular or prismatic crystals and a random orientation of the other crystallographic axes produces a lineation petrofabric. In a pole figure, this CPO is usually expressed by point maxima for the long axis and a circular/girdle distribution of the other axes. Such a fabric develops in dominantly constrictional flows whereby $\sigma1=\sigma2>>\sigma3$. Such a CPO is expected to be generated locally in transpressional flow (Fossen & Tikoff, 1998; Tikoff & Fossen, 1999), where flow is partitioned into constrictional and simple shear flow. Another scenario would be a plug flow (Johnson, 1970), as occurs in lava tubes (Peterson *et al.*, 1994). This fabric is not observed in any of the nakhlites studied here.

Many natural examples have mixtures of these end-member CPOs. Most importantly, within any flow that has both a flattening, pure shear component and a directional, simple shear

component, a foliation is often produced alongside a lineation (Merle, 1998; Iezzi & Ventura, 2002). In a subaerial magmatic flow, both rotational (simple shear) and non-rotational, flattening (pure shear) are likely to occur, where the simple shear component dominates close to the shear plane (e.g., Merle, 1998 Figure 8; Iezzi & Ventura, 2002). This shear plane, in the case of a subaerial lava flow, is situated at the base of the flow in contact with the bedrock. The magnitude of the pure shear component depends on the effect of overburden causing compaction, as well as on the timescales of melt/mesostasis cooling and crystallisation. Flow dominated by simple shear favours a more pronounced point maxima/lineation, whereas flow dominated by pure shear favours girdle distribution/foliation. In a divergent flow (i.e., flowing lava that spreads out), the volume of flow with a significant flattening component is relatively large and close to the bedrock, whereas constrictional flow is dominant close to the top of the lava. Such a flow mixture is consistent with the petrofabrics observed in Governador Valadares and Nakhla (Figure 2, 3).

In magmatic systems that contain both phenocrysts and matrix (i.e., melt, mesostasis), the volume ratio of these two components further influences the strength of a CPO. At low ratios (i.e., large amounts of matrix and few phenocrysts), the strength will oscillate, but may temporarily be high (Jezek *et al.,* 1996; Piazolo *et al.,* 2002), whereas at high phenocryst/matrix ratios (e.g. where >40% of phenocrysts interact with each other) the CPO strength is more stable but usually less pronounced (Ildefonse *et al.,* 1992). Therefore, in phenocryst-rich lavas such as some of the nakhlites interactions between adjacent phenocrysts can inhibit rotation and so hinder fabric development. This process may cause substantial variations in fabric strength between and within nakhlites, or even produce some regions on the hand specimen to outcrop scale that completely lack a fabric (Ildefonse *et al.*, 1992; Iezzi & Ventura, 2002).

4.3. Magmatic environments for the four nakhlites

All four nakhlites have petrofabrics (i.e. non-random 3D-SPOs and CPOs). This indicates that their parent magmas were subject to non-chaotic flow and so cannot have cooled in a turbulent regime.

The 2D-SPO data suggest that the petrofabrics of Nakhla and Governador Valadares (no apparent 2D-SPO, Figures 2B, 3B) are different to MIL 03346 and Lafayette (strong 2D-SPO; Figures 4B, 5B). However, due the arbitrary orientations of the thin sections, 2D-SPO cannot be solely used to reliably distinguish nakhlite fabrics and petrographic relationships. EBSD pole figures, PGR plots and J-index metrics indicate that all of the nakhlites have a weak to moderate girdle maxima defined by the alignment of the long <c> crystal axes of augite phenocrysts within a plane, which represents a magmatic foliation (Figures 2-6). Additionally, EBSD crystal pole figures and PGR plots separate the nakhlites into two sets: Nakhla + Governador Valadares, and Lafayette + MIL 03346. Nakhla and Governador Valadares have a weak but clear <c> crystal axis lineation, contained within the <c> crystal axis foliation (Figures 2C, 3C, 6). The EBSD pole figure for MIL 03346 is suggestive of a <c> crystal axis lineation contained within the <c> crystal axis foliation (Figure 4), although such a fabric is not revealed by the PGR ternary diagram (Figure 6). By contrast, both the EBSD pole figures and PGR data of Lafayette show only a crystal foliation. Therefore, the presence of a <c> crystal axis lineation petrofabric distinguishes Nakhla and Governador Valadares from MIL 03346 and Lafayette, in that Nakhla and Governador Valadares show a <c> crystal axis lineation. This said, the PGR values of all three crystallographic axes of Lafayette show that its crystal foliation is much weaker than the other three nakhlites, as

evidenced by a lower G value in the PGR plot (Figure 6). Thus, the four samples should be divided into three sets from their CPO petrofabrics.

The M-index results suggest that all samples have a random fabric, which contradicts the other quantitative petrographic metrics described above. This apparent discrepancy can be readily explained because the M-index gives equal weighting to the three major crystallographic axes. Thus, the augite crystals will have a low M-index because their <c> axis is aligned to form a weak to moderate girdle fabric whereas the <a> and <b> aces are not (Figure 6); the M-index value for the whole rock is therefore much lower than expected from the observed <c> crystal axis fabric. Based on all other data (i.e., J-index, pole figure, PGR), we conclude that these nakhlites contain at least a <c> crystal axis girdle maxima and that Nakhla and Governador Valadares are likely to be distinct from MIL 03346, and are certainly different to Lafayette.

The common crystallographic petrofabrics of Nakhla and Governador Valadares (Figures 2, 3) mirror other petrologic similarities. These two meteorites have a near identical modal mineralogy, a similar major and minor element geochemistry, and comparable cooling rates as inferred from the thickness of Fe-rich rims in olivine and the width of plagioclase laths (Treiman, 2005; Corrigan *et al.*, 2015; Udry & Day, 2018 and references therein). These similarities therefore suggest that the two rocks cooled and crystallised in a comparable regime and from a compositionally similar melt and therefore, these two nakhlites may sample the same lava flow. This hypothesis could be tested by high-resolution $^{40}Ar/^{39}Ar$ geochronology as used by Cohen *et al.* (2017) to corroborate the quantitative textural and geochemical analyses of these meteorites that suggest Nakhla and Governador Valadares formed in the same flow (Udry and Day 2018). Our finding of a weak-moderate

crystallographic foliation and lineation in Nakhla and Governador Valadares is consistent with pure shear, with a small but distinct component of simple shear. Such forces are suggestive of a hyperbolic flow regime as observed mainly in subaerial lava flows on Earth (Merle, 1998; Iezzi & Ventura, 2002).

MIL 03346 and Lafayette have little or no crystallographic lineation, and display moderate and weak <c> crystal axis foliations, respectively. These crystallographic petrofabrics and inferred 3D-SPO's imply a regime strongly dominated by pure shear with gravitational settling of crystals, such as a lava lake, sill or stagnant regime of a lava flow. One could also envisage a spreading lava flow, where a pure shear/constrictional stress regime dominated. Differences between these two meteorites in the strength of their <c> crystal axis foliation and inferred 3D-SPO, indicates that they were emplaced under contrasting conditions, although the higher phenocryst to matrix ratio of Lafayette relative to MIL 03346 may have also contributed to its weaker CPO fabric strength. This conclusion is consistent with their $^{40}Ar/^{39}Ar$ ages, which differ by ~70 Ma (Cohen *et al.*, 2017), and previous geochemical and textural analysis of these rocks (Udry and Day 2018) which suggest that they formed in discrete magmatic events.

4.4. Relative positions within each individual magma body

The chemical zoning in nakhlite olivine shows that out of the four meteorites studied here, MIL 03346 cooled relatively rapidly, whereas Lafayette cooled much more slowly (Treiman, 2005; Day *et al.*, 2006; Mikouchi *et al.*, 2012). Cooling rate can be used as a proxy for former position of the meteorite within its parent magmatic body (i.e., MIL 03346 was from close to the top of its magmatic unit and Lafayette crystallised at a greater depth within its magmatic unit where heat loss was slower; Treiman, 2005; Day *et al.*, 2006; Mikouchi *et al.*, 2012).

Petrofabric results are also consistent with such relative positions within their discrete magma bodies. Specifically, the weaker CPO and lower proportion of mesostasis of Lafayette relative to MIL 03346 implies that Lafayette cooled at the base of a relatively thick magma body, where the compaction of crystals during settling expelled melt, and the resulting high abundance of phenocrysts inhibited CPO and 3D-SPO fabric development (Ildefonse *et al.*, 1992; Iezzi & Ventura, 2002). These conclusions are also consistent with the equilibrated composition of the olivine and pyroxene phenocrysts and crystalline nature of the mesostasis described previously (Day *et al.*, 2006). The greater CPO strength of MIL 03346 (Figure 6) and its high abundance of mesostasis (Day *et al.*, 2006) suggests that it crystallised rapidly in the upper part of a thick lava flow, or alternatively the lower part of a flattening thin flow. Under these conditions the expulsion of mesostasis due to crystal compaction would have been minimised so that 3D-SPO fabric development (inferred from CPO) would not be inhibited. This scenario is again consistent with previous models (Day *et al.*, 2006) based on the meteorite's disequilibrium mineral textures, such as rimmed olivine and pyroxene, and evidence for rapid cooling from the fine grained-glassy mesostasis.

Lafayette and MIL 03346 must sample distinct magmatic units as they are temporally separated by ~70 Ma (Cohen *et al.*, 2017), while their petrofabrics are consistent with a similar emplacement mechanism within cumulate flows (Lentz *et al.*, 1999; Mikouchi *et al.*, 2003; Treiman, 2005; Day *et al.*, 2006; Mikouchi *et al.*, 2012; Udry & Day, 2018). Thus, the volcanic system that generated the nakhlites had several episodes of similar volcanic activity producing similar igneous units over at least 70 Ma.

Nakhla and MIL 03346 are temporally indistinguishable (Cohen *et al.*, 2017) despite having a distinct CPO petrofabric (Figure 6, Treiman, 2005; Day *et al.*, 2006; Hallis *et al.*, 2012;

Corrigan *et al.*, 2015; Udry & Day, 2018). There are two ways to reconcile this apparent contradiction. One is that they formed in two different magmatic environments and events, which cannot be resolved by $^{40}Ar/^{39}Ar$ geochronology. Alternatively, if Nakhla and MIL 03346 were contemporaneous their different petrofabrics could be explained by their parent lava being internally complex, for example exhibiting both hyperbolic flow and gravity settling (e.g. a lava flow feeding into a lava lake). Such internal heterogeneity could have been developed over length scales of less than 3 km (i.e., as constrained by the size of the crater formed during the nakhlite impact-ejection event, Fritz *et al.*, 2005). Similar textural heterogeneity has been described in terrestrial lava flows such as Theo's flow (Lentz *et al.*, 1999) as well as sills and dykes (Shelley, 1985; Wada, 1992). Locally these 3D-SPO fabrics inferred from CPO may be stronger or weaker through grain-grain interactions during flow that result in episodic weakening and/or strengthening of the fabric (Ildefonse *et al.*, 1992; Iezzi & Ventura, 2002; Jezek *et al.*, 1996; Piazolo *et al.*, 2002) consistent with the higher mesostasis/phenocryst ratio of MIL 03346 relative to Nakhla (Treiman, 2005; Day *et al.*, 2006; Corrigan *et al.*, 2015; Udry & Day, 2018). For these specific meteorites, the higher mesostasis abundance of MIL 03346 has been suggested to form as a quench cooled break out from the front of a lava flow (Hallis *et al.*, 2012). Such a rapid unidirectional forcing might generate the gravity settling CPO texture we observe in MIL 03346 (Figures 4, 6). Nakhla cooled over a longer time period, evidenced by the equilibrated textures of the phenocrysts (Treiman, 2005), and so likely formed within the main portion of the flow, and therefore had time to generate the hyperbolic flow CPO fabric (Figures 2, 6). The scenario above is however, but one solution of many that can occur in complex volcanic systems.

The presence or absence of crystallographic lineations and/or foliations, coupled with equivalent 3D-SPO development (inferred from the CPO data), can be used to identify the

relative orientations of the Martian surface and the approximate line of flow of the parent magmas of these meteorites. Provided that the 3D shape orientation of augite phenocrysts in the nakhlites is an expression of a gravity driven processes, the 3D-SPO/CPO foliation plane would be sub-parallel to the Martian surface. As the four nakhlites all exhibit a <c> crystal axis foliation, the trace of this girdle is within 10-20° the plane of surface of Mars (the red dashed line in Figures 2C, 3C, 4C, and 5C).

In the presence of a significant simple shear component, any 3D-SPO lineation (inferred from the CPO) generated would define the line along which the parent lava flowed. Nakhla and Governador Valadares exhibit such a lineation in their <c> crystal axes and as such represents the line of magmatic flow in these rocks (the white dashed circle in the <c> axis in Figure 2C and 3C). However, care must be taken when interpreting flow lines from 3D-SPO/CPO lineations, as models suggest that such lineations form at a slight angle (<20°) to the flow direction (Passchier, 1982). Using these crystallographic petrofabrics to produce new thin sections that are parallel and perpendicular to these fabrics would enable identification of other way up criteria and the direction of the gravitational force or direction of flow, and as such the meteorites' position relative to the Martian surface.

4.5. Geological settings for the origin of the nakhlites.

The nakhlite meteorites are, in a broad sense, petrographically similar (Treiman, 2005) as they have the same general composition and general matrix-phenocryst characteristics. However, there are distinct petrographic differences between them and within individual meteorites, such as mesostasis abundance, phenocryst size, and reaction rim thickness representing different phenocryst equilibrium (e.g., Mikouchi *et al.*, 2003; Corrigan *et al.*, 2015; Udry & Day, 2018). Furthermore, previous reports of the presence or absence of 2D-

SPO fabrics within the nakhlite meteorites are contradictory. Some studies have described foliations and even lineations (Bunch & Reid, 1975; Berkley *et al.*, 1980; Mikouchi *et al.*, 2003), while others report no distinct fabric, maybe because they used image analysis that cannot extract CPO information (Lentz *et al.*, 1999; Udry & Day, 2018). Our results demonstrate that the nakhlites do preserve 3D-SPO petrofabrics inferred from CPO, and the strength and type of fabrics observed varies between meteorites owing to contrasting emplacement mechanisms. In turn, these findings support the suggestion that the nakhlites are from different magmatic units (Cohen *et al.*, 2017).

There is an ongoing debate regarding the emplacement environment of these rocks relative to the Martian surface. Both subaerial flows and subsurface sills have been suggested (Treiman, 2005) but it is unclear how these environments could be distinguished. For example, cooling rate could be used, but it is also a function of the thickness of a lava flow/intrusion, and in the case of an intrusion, the depth of emplacement is also a factor. Even the petrofabrics indicative of flow described in this study, while more likely to have formed within a subaerial lava flow, are not a unique signature; similar petrofabrics have been reported in parts of terrestrial sills and dykes (Shelley, 1985; Wada, 1992). The fact that the nakhlites have been ejected from Mars in an impact can also be used to constrain emplacement environment. Rocks will be excavated from depths of up to 1/5 of the impactor diameter (Artemieva & Ivanov, 2004) so that a bolide producing a 10 km crater would eject rocks from a maximum depth of ~65 m (Cohen *et al.*, 2017). These shallow levels would favor lava flows as intrusions would be more abundant at depth beneath the volcanic edifice (assuming low rates of erosion). The nakhlite's mild shock metamorphism also favors shallow ejection depths (Artemieva & Ivanov, 2004; Fritz *et al.*, 2005; Treiman, 2005), although again this is not a unique requirement. Conversely, the phenocryst/mesostasis ratio of the nakhlites is generally

above the point of critical crystallinity (~55%) that would inhibit eruption and flow of these magmas and would indicate emplacement as a sill rather than a lava flow. However, our CPO data indicate that some mesostasis may have been lost through compaction of phenocrysts during simple and pure shear – an observation which may indicate that these lavas were once more mesostasis-rich. This would imply that sub-aerial emplacement remains plausible.

The variety of petrofabrics present in the nakhlite meteorites suggest a diverse range of magmatic emplacement mechanisms and lava thickness at the nakhlite source volcano/volcanoes. Governador Valadares and Nakhla display both pure/flattening and simple shear flow components consistent with subaerial flow, while MIL 03346 and Lafayette likely formed at the top and bottom, respectively, of a highly pure shear/flattening dominated regime consistent with stagnant lava lake. The emplacement mechanisms inferred for these meteorites would mean that these fabrics would be transient (rapidly being created and destroyed over a cm-m scale). Therefore, some regions within a given nakhlite meteorite may have no distinct crystallographic fabric, which may explain the apparent absence of 2D-SPO petrofabrics found in previous nakhlite studies (e.g., Udry & Day, 2018). This possibility, means care must be taken when extrapolating petrofabrics observed in one thin section as representative of the whole rock and inferring formation environment. However, this could readily be tested by EBSD analysis of the samples used in previous studies and ideally expanded to include several sections from different portions of each meteorite and/or paired stones.

All cosmogenic exposure measurements undertaken on the nakhlites indicate that these rocks were ejected from the Martian surface in a single impact event at 11 Ma (Benn & Allard, 1989; Nyquist *et al.*, 2001; Treiman, 2005; Cohen *et al.*, 2017). The diversity of petrofabrics

observed here and reported elsewhere implies that the impact site is at an edifice with prolonged subaerial magmatic activity including lava flows of variable thickness, as well as loci of gravitation crystal settling and melt expulsion. Such a complex volcanic setting exhibited by the nakhlite petrofabrics may potentially rule out 'simpler' geological terrains on Mars as candidates for the Nakhlite launch site.

5. Conclusions

Identifying the launch site for the nakhlite meteorites is critical for calibrating the age of the Martian surface. Through petrographic analysis we can understanding how these nakhlite meteorites were emplaced to constrain the geological setting and terrain in which they formed. Thus, providing tighter constraints on the possible terrains sampled by the Nakhlite source crater. In this study, large area EBSD mapping of four Martian igneous rocks has revealed a diversity of 3D-SPO petrofabrics inferred from CPO data that indicate cooling and crystallisation in two distinct magmatic environments.

1) Nakhla and Governador Valadares. These meteorites have similar foliation and lineation petrofabrics consistent with emplacement in a magmatic flow – either a lava flow, or a sill that was undergoing magma flow.
2) MIL 03346 and Lafayette exhibit only a foliation consistent with crystal settling in either a quiescent magmatic system or the flattening regime in the lower parts of a spreading lava flow. The substantially lower fabric strength in Lafayette is likely due to phenocryst abundance inhibiting fabric development. The distinct crystallisation ages of these two meteorites indicate that at least two spreading lava flows were generated from the same region of the Martian crust over 70 Ma.

These petrofabrics constrain both the line of flow and the plane of the Martian surface. The two distinct modes of emplacement imply a complex magmatic system in the vicinity of the nakhlite ejection site. We propose that the crater formed during impact ejection of the nakhlites is superimposed upon a complex volcanic edifice. Thus, any ~11 Ma crater candidates for the nakhlite source must fulfil this criterion and craters superimposed on relatively simple volcanic terrains are relatively poor candidates for the nakhlites. These new petrographic constraints can aid in focusing the search for the elusive nakhlite source crater. The approach outlined here can also be applied to understand other volcanic systems on Mars and terrestrial planets in the solar system.

6. Acknowledgements

We thank the following institutions for providing the meteorite samples: Smithsonian Institute, NASA Meteorite Working Group, Natural History Museum London (loan of Governador Valadares), Macovich Collection, The Western Australia Museum, and the Japanese Antarctic Meteorite Research Centre. US Antarctic meteorite samples are recovered by the Antarctic Search for Meteorites (ANSMET) program which has been funded by NSF and NASA, and characterised by the Department of Mineral Sciences of the Smithsonian Institution and Astromaterials Acquisition and Curation Office at NASA Johnson Space Centre. This work was funded by the Science and Technology Facilities Council through grants ST/N000846/1 and ST/H002960/1 to M.R.L). The authors acknowledge the facilities, and the scientific and technical assistance, of the Australian Microscopy & Microanalysis Research Facility at the Centre for Microscopy, Characterisation and Analysis, University of Western Australia and the Imaging Spectroscopy and Analysis Centre, University of Glasgow. The authors would also like to

thank Prof. Arya Udry, one anonymous reviewer and handling editor Prof. Tamsin Mather for their invaluable comments and suggestions to improve this manuscript.

Figure Captions

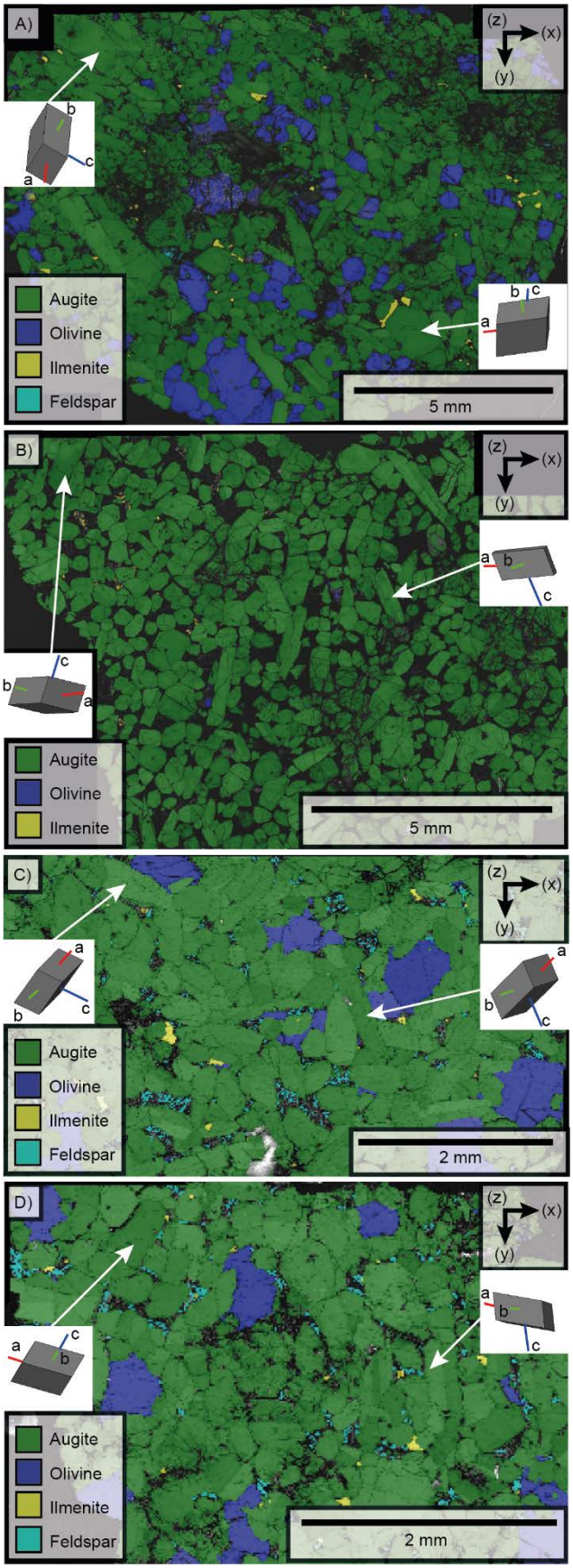
A)
(z)
(x)
(y)
b
c
a
Augite
Olivine
Ilmenite
Feldspar
5 mm
B)
(z)
(x)
(y)
a
b
c
c
b
a
Augite
Olivine
Ilmenite
5 mm
C)
(z)
(x)
(y)
a
b
c
a
b
c
Augite
Olivine
Ilmenite
Feldspar
2 mm
D)
(z)
(x)
(y)
a
b
c
c
a
b
Augite
Olivine
Ilmenite
Feldspar
2 mm

Figure 1

EBSD maps of Lafayette (A), MIL 03346 (B), Governador Valadares (C), and Nakhla (D), highlighting different mineral phases by discrete colours (see key). The insets are 3D visualisations of selected crystals, which reveal that crystal shapes correlate with crystallographic orientations whereby the long shape axis corresponds to the <c> crystal axis and the short shape axes to the crystallographic <a> and <b> crystal axes. In addition, it is clear that grain boundaries are commonly formed by low index planes (i.e., facets); hence grains represent phenocrysts.

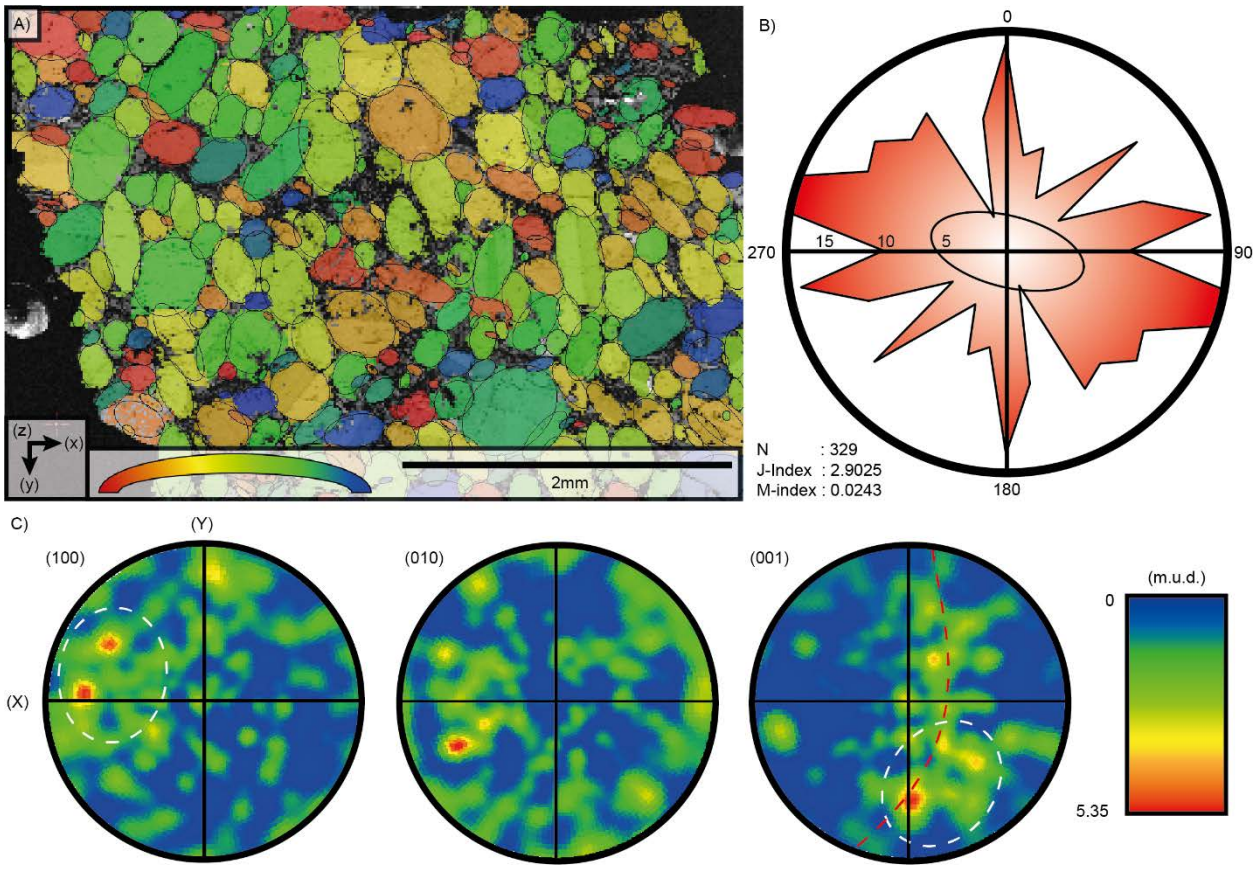

Figure 2

Quantitative EBSD characterisation of Nakhla. A) EBSD map, colour coded using the 2D-SPOs of augite crystals. B) Rose diagram of long axis 2D-SPOs. C) Contoured pole figures of the main crystallographic axes <a>, <b> and <c>. The red dashed line represents the 3D-SPO foliation plane inferred from the CPO, and the plane of the Martian surface, whereas the white dashed lines represent point maxima; in the <c> crystal axis the point maxima represent the line of magmatic flow. M and J index values are listed with the pole figures: N denotes the number of grains measured: m.u.d. = multiples of uniform density.

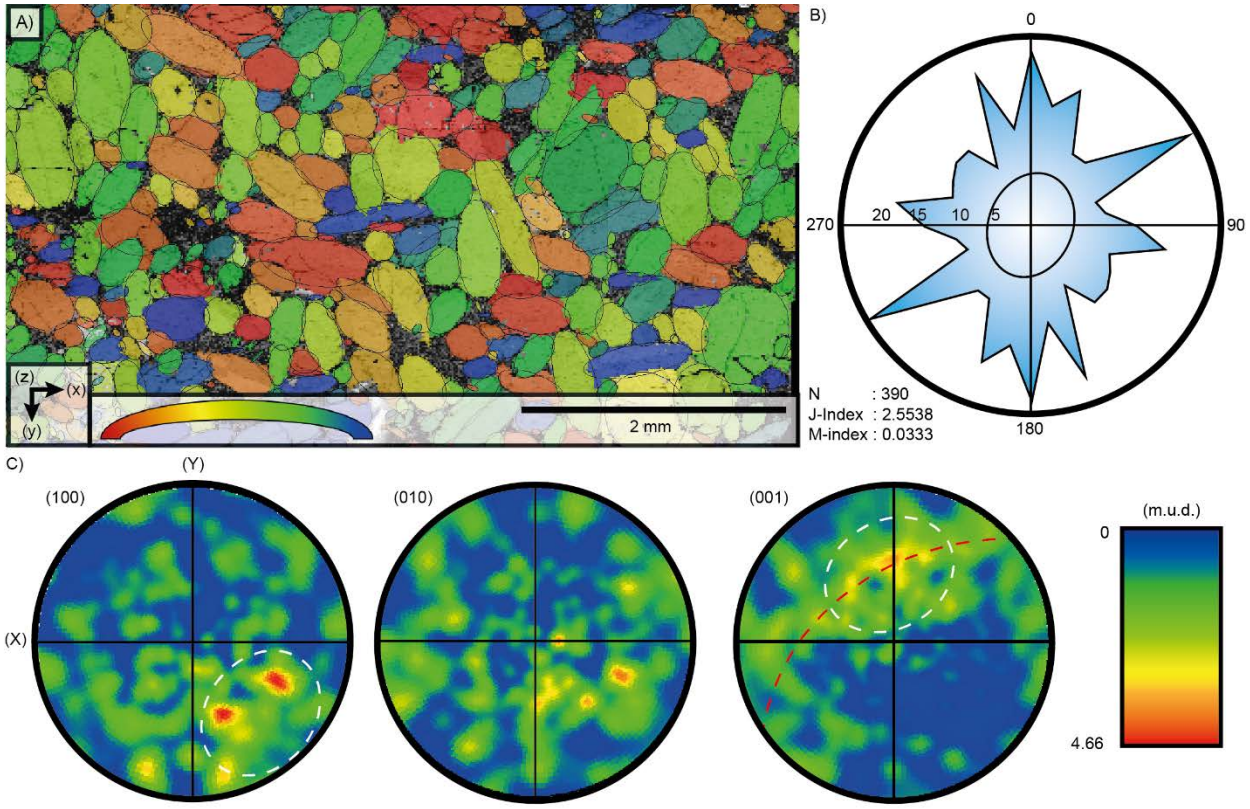

Figure 3

Quantitative EBSD characterisation of Governador Valadares. A) EBSD map, colour coded using the 2D-SPOs of augite crystals. B) Rose diagram of long axis 2D-SPOs. C) Contoured pole figures of the main crystallographic axes <a>, <b> and <c>. The red dashed line represents the 3D-SPO foliation plane inferred from the CPO, and the plane of the Martian surface, whereas the white dashed lines represent point maxima; in the <c> crystal axis the point maxima represents the line of magmatic flow. M and J index values are listed with the pole figure: N denotes the number of grains measured: m.u.d. = multiples of uniform density.

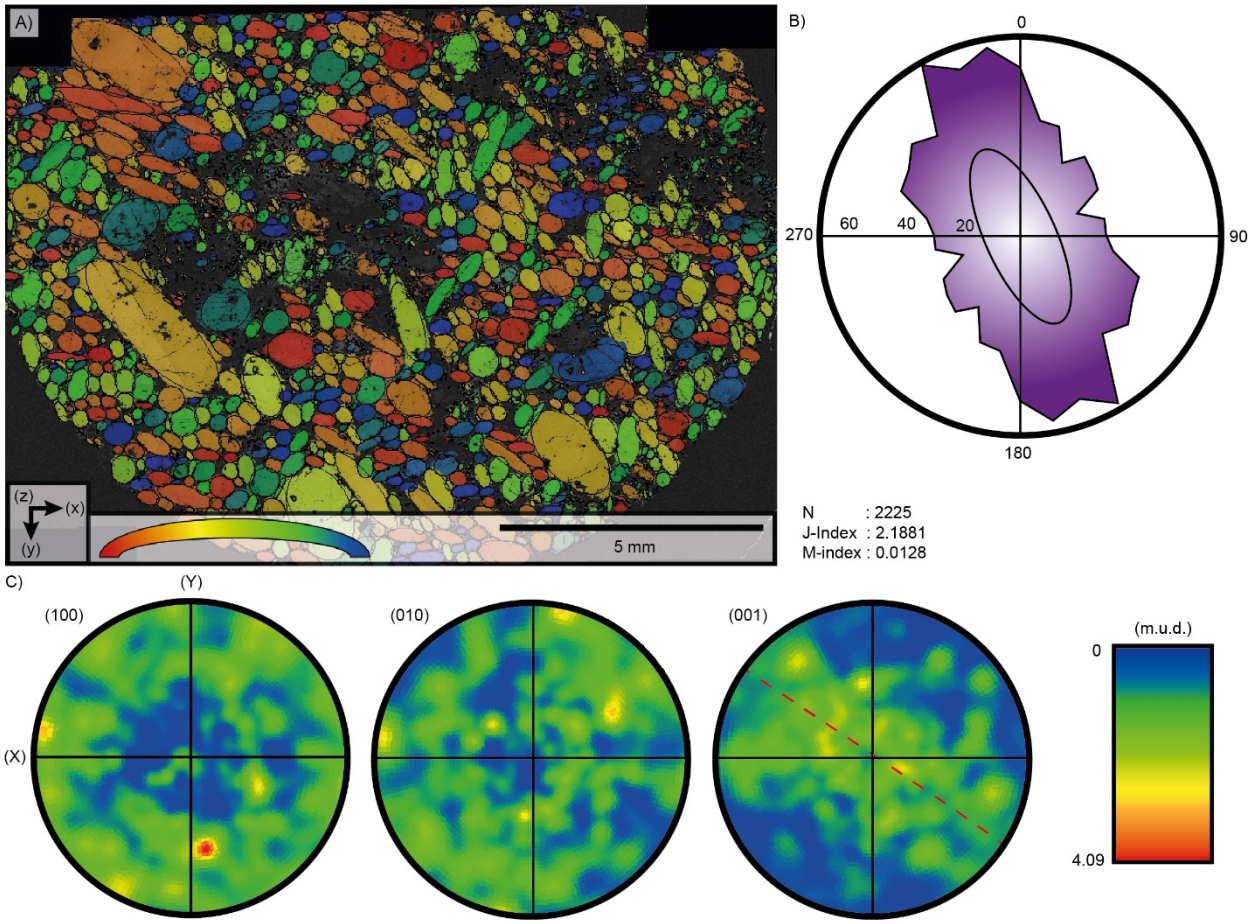

Figure 4

Quantitative EBSD characterisation of Lafayette. A) EBSD map, colour coded using the 2D-SPOs of augite crystals. B) Rose diagram of long axis 2D-SPOs. C) Contoured pole figures of the main crystallographic axes <a>, <b> and <c>. The red dashed line represents the 3D-SPO foliation plane inferred from the CPO data, and the plane of the Martian surface. M and J index values are provided with the pole figure: N denotes the number of grains measured: m.u.d. = multiples of uniform density.

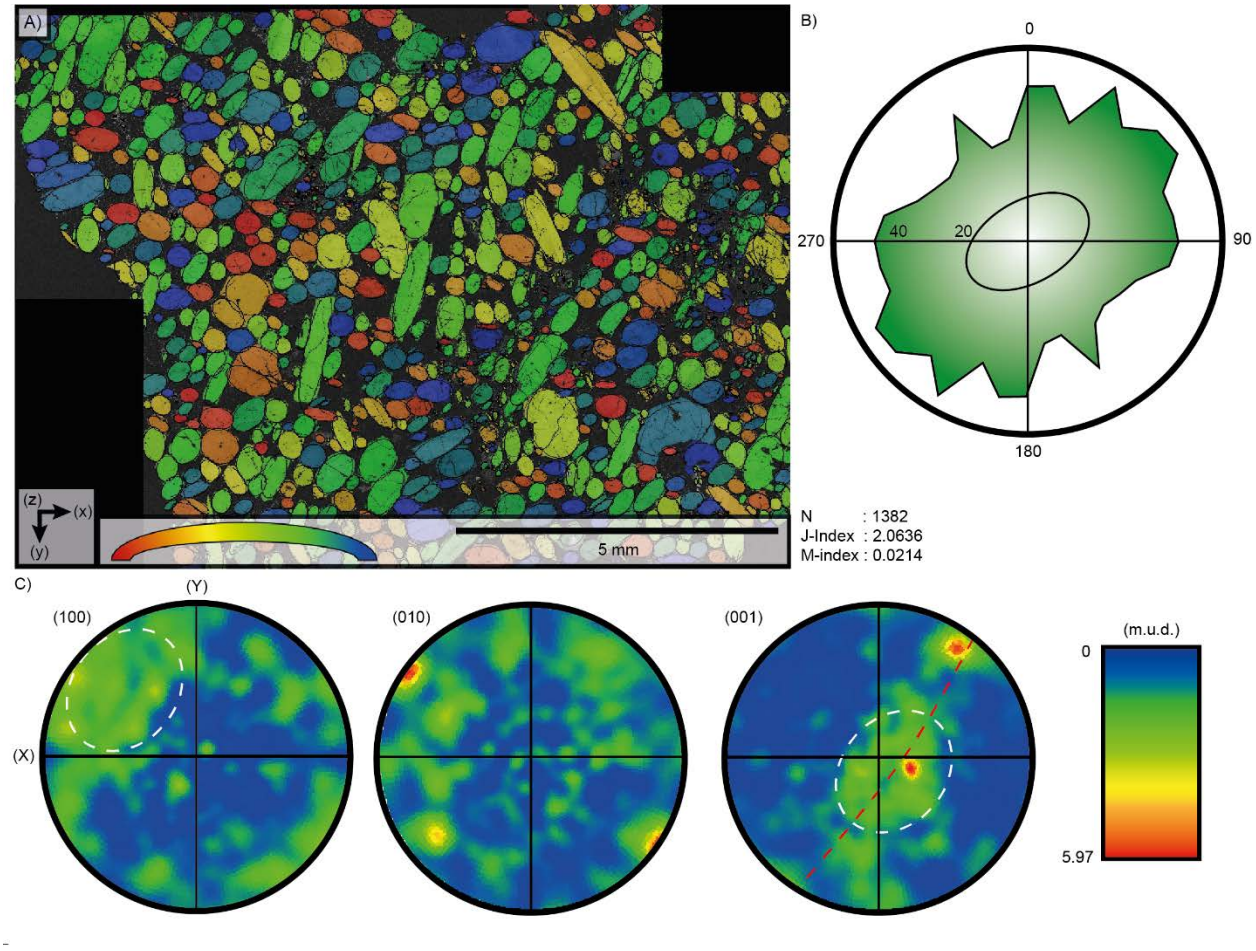

Figure 5

Quantitative EBSD characterisation of MIL 03346. A) EBSD map, colour coded using the 2D-SPOs of augite crystals. B) Rose diagram of long axis 2D-SPOs. C) Contoured pole figures of the main crystallographic axes <a>, <b> and <c>. The red dashed line represents the 3D-SPO foliation plane inferred from the CPO data, and the plane of the Martian surface, whereas the white dashed lines represent point maxima; in the <c> crystal axis the point maxima represents the line of magmatic flow. M and J index values are provided with the pole figure: N denotes the number of grains measured: m.u.d. = multiples of uniform density.

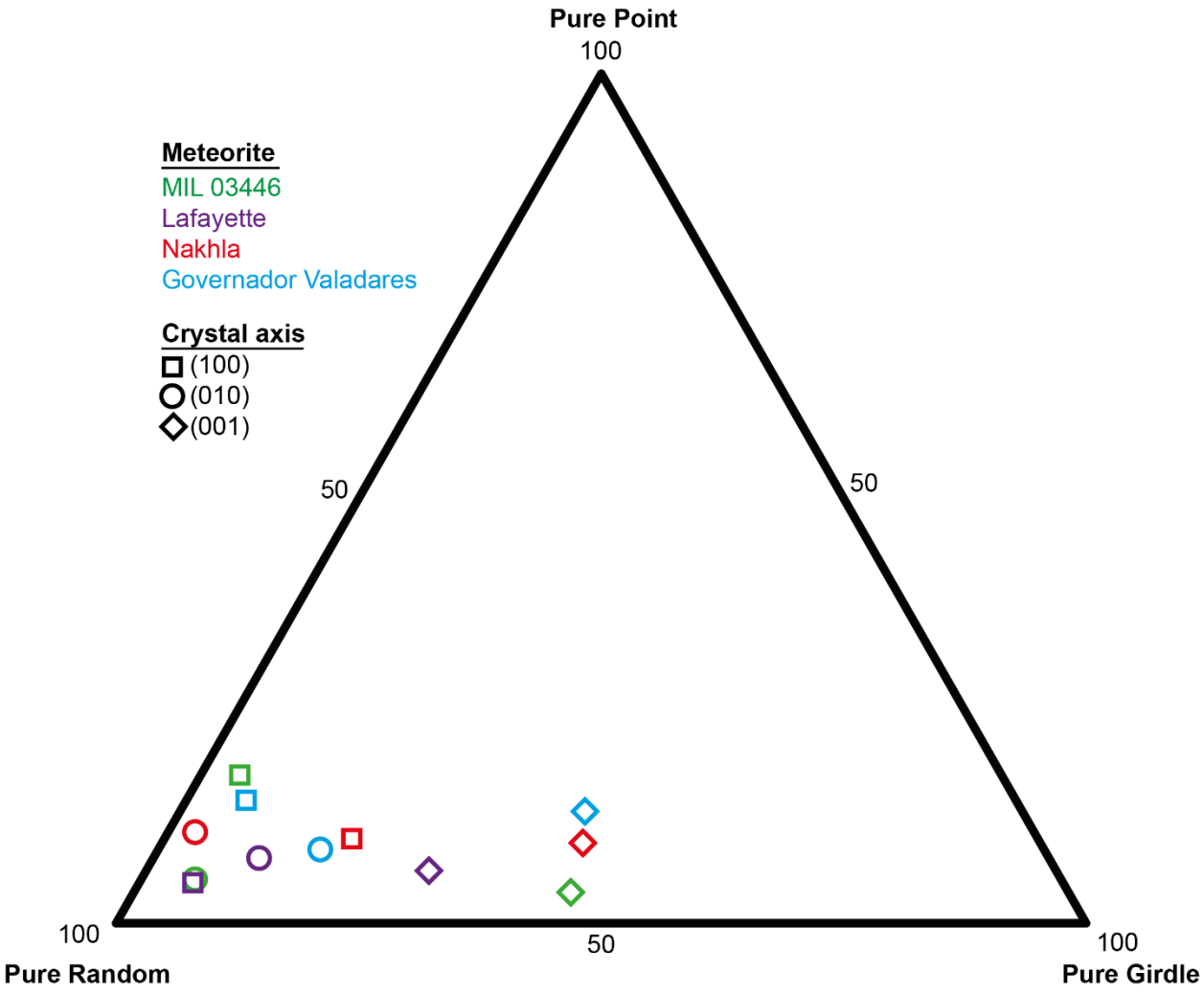

Figure 6

Ternary diagram of the dominant 3D-SPO crystal fabrics inferred from the CPO data (pure random, pure girdle, pure point maxima) in Nakhla, Governador Valadares, Lafayette, and MIL 03346. We infer a random fabric for $R > 90$ %. P or G values between 10-30 % are interpreted as weak fabrics, 30-50% as moderate fabrics and >50% as a strong fabric. There is a moderate to strong girdle in the (001) of all meteorites, and a weak point in the (001) of Governador Valadares and Nakhla and the (100) axis of all studied nakhlites except Lafayette.

REFERENCES CITED

Artemieva, N., & Ivanov, B. (2004). Launch of Martian meteorites in oblique impacts. *Icarus, 171*(1), 84-101.

Ashworth, J., & Hutchison, R. (1975). Water in non-carbonaceous stony meteorites. *Nature, 256*(5520), 714-715.

Bachmann, F., Hielscher, R., Jupp, P. E., Pantleon, W., Schaeben, H., & Wegert, E. (2010). Inferential statistics of electron backscatter diffraction data from within individual crystalline grains. *Journal of Applied Crystallography, 43*(6), 1338-1355.

Bascou, J., Camps, P., & Dautria, J. M. (2005). Magnetic versus crystallographic fabrics in a basaltic lava flow. *Journal of Volcanology and Geothermal Research, 145*(1-2), 119-135.

Benn, K., & Allard, B. (1989). Preferred mineral orientations related to magmatic flow in ophiolite layered gabbros. *Journal of Petrology, 30*(4), 925-946.

Berkley, J., Keil, K., & Prinz, M. (1980). Comparative petrology and origin of Governador Valadares and other nakhlites. *11th Lunar and Planetary Science Conference*, 1089-1102.

Bestmann, M., & Prior, D. J. (2003). Intragranular dynamic recrystallization in naturally deformed calcite marble: diffusion accommodated grain boundary sliding as a result of subgrain rotation recrystallization. *Journal of Structural Geology, 25*(10), 1597-1613.

Bhattacharyya, D. (1966). Orientation of mineral lineation along the flow direction in rocks. *Tectonophysics, 3*(1), 29-33.

Bogard, D. D., & Johnson, P. (1983). Martian gases in an Antarctic meteorite? *Science, 221*(4611), 651-654.

Boiron, T., Bascou, J., Camps, P., Ferré, E., Maurice, C., Guy, B., Gerbe, M.-C., & Launeau, P. (2013). Internal structure of basalt flows: insights from magnetic and crystallographic fabrics of the La Palisse volcanics, French Massif Central. *Geophysical Journal International, 193*(2), 585-602.

Borthwick, V. E. and Piazolo S., 2010, Post-deformational annealing at the subgrain scale: Temperature dependant behaviour revealed by in-situ heating experiments on deformed single crystal halite, *Journal of structural Geology*, 32(7), 982-996.

Bridges, J. C., Hicks, L. J., & Treiman A. H., (2019), Carbonates on Mars in *Volatiles in the Martian Crust*, 1st Edition, Eds Filiberto and Schwenzer, 426.

Bunch, T., & Reid, A. M. (1975). The nakhlites Part I: Petrography and mineral chemistry. *Meteoritics & Planetary Science, 10*(4), 303-315.

Bunge, H.-J. (2013). *Texture analysis in materials science: mathematical methods*: Elsevier.

Changela, H., & Bridges, J. (2010). Alteration assemblages in the nakhlites: Variation with depth on Mars. *Meteoritics & Planetary Science, 45*(12), 1847-1867.

Cohen, B., Mark, D. F., Cassata, W. S., Lee, M. R., Tomkinson, T., & Smith, C. L. (2017). Taking the Pulse of Mars via $^{40}Ar/^{39}Ar$ Dating of a Plume-Fed Volcano. *Nature communications, 8*(640).

Corrigan, C. M., Velbel, M. A., & Vicenzi, E. P. (2015). Modal abundances of pyroxene, olivine, and mesostasis in nakhlites: Heterogeneity, variation, and implications for nakhlite emplacement. *Meteoritics & Planetary Science, 50*(9), 1497-1511.

Day, J. M. D., Taylor, L. A., Floss, C., & McSween, H. Y. (2006). Petrology and chemistry of MIL 03346 and its significance in understanding the petrogenesis of nakhlites on Mars. *Meteoritics & Planetary Science, 41*(4), 581-606.

Fossen, H., & Tikoff, B. (1998). Extended models of transpression and transtension, and application to tectonic settings. *Geological Society, London, Special Publications, 135*(1), 15-33.
Fritz, J., Artemieva, N., & Greshake, A. (2005). Ejection of Martian meteorites. *Meteoritics & Planetary Science, 40*(9-10), 1393-1411.
George, R. P. (1978). Structural petrology of the Olympus ultramafic complex in the Troodos ophiolite, Cyprus. *Geological Society of America Bulletin, 89*(6), 845-865.
Hallis, L., Taylor, G., Nagashima, K., Huss, G., Needham, A., Grady, M., & Franchi, I. (2012). Hydrogen isotope analyses of alteration phases in the nakhlite martian meteorites. *Geochimica et Cosmochimica Acta, 97*, 105-119.
Harvey, R. P., & McSween, H. Y. (1992). Petrogenesis of the nakhlite meteorites: Evidence from cumulate mineral zoning. *Geochimica et Cosmochimica Acta, 56*(4), 1655-1663.
Hicks, L. J., Bridges, J. C., &Gurman, S.J. (2014) Ferric saponite and serpentine in the nakhlite martian meteorites, *Geochimica et Cosmochimica Acta*, 136, 194-210.
Iezzi, G., & Ventura, G. (2002). Crystal fabric evolution in lava flows: results from numerical simulations. *Earth and Planetary Science Letters, 200*(1-2), 33-46.
Ildefonse, B., Sokoutis, D., & Mancktelow, N. S. (1992). Mechanical interactions between rigid particles in a deforming ductile matrix. Analogue experiments in simple shear flow. *Journal of Structural Geology, 14*(10), 1253-1266.
Ismaıl, W. B., & Mainprice, D. (1998). An olivine fabric database: an overview of upper mantle fabrics and seismic anisotropy. *Tectonophysics, 296*(1-2), 145-157.
Jackson, E. (1961). *Primary textures and mineral associations in the ultramafic zone of the Stillwater complex, Montana* (2330-7102).
Ježek, J., Schulmann, K., & Segeth, K. (1996). Fabric evolution of rigid inclusions during mixed coaxial and simple shear flows. *Tectonophysics, 257*(2-4), 203-221.
Johnson, A. M. (1970). *Physical processes in geology: A method for interpretation of natural phenomena; intrusions in igneous rocks, fractures, and folds, flow of debris and ice*: Freeman, Cooper.
Lentz, R. F., Taylor, G., & Treiman, A. (1999). Formation of a Martian pyroxenite: A comparative study of the nakhlite meteorites and Theo's Flow. *Meteoritics & Planetary Science, 34*(6), 919-932.
Merle, O. (1998). Internal strain within lava flows from analogue modelling. *Journal of Volcanology and Geothermal Research, 81*(3-4), 189-206.
Mikouchi, T., Koizumi, E., Monkawa, A., Ueda, Y., & Miyamoto, M. (2003). Mineralogy and petrology of Yamato 000593: Comparison with other Martian nakhlite meteorites. *Antarctic Meteorite Research, 16*, 34-57.
Mikouchi, T., Makishima, J., Kurihara, T., Hoffmann, V., & Miyamoto, M. (2012). Relative burial depth of nakhlites revisited. *43rd Lunar and Planetary Science Conference*, 2363.
Nyquist, L., Bogard, D., Shih, C.-Y., Greshake, A., Stöffler, D., & Eugster, O. (2001). Ages and geologic histories of Martian meteorites *Chronology and evolution of Mars* (pp. 105-164): Springer.
Passchier, C. (1982). Pseudotachylyte and the development of ultramylonite bands in the Saint-Barthelemy Massif, French Pyrenees. *Journal of Structural Geology, 4*(1), 69-79.
Paterson, S. R., Fowler Jr, T. K., Schmidt, K. L., Yoshinobu, A. S., Yuan, E. S., & Miller, R. B. (1998). Interpreting magmatic fabric patterns in plutons. *Lithos, 44*(1-2), 53-82.
Peterson, D. W., Holcomb, R. T., Tilling, R. I., & Christiansen, R. L. (1994). Development of lava tubes in the light of observations at Mauna Ulu, Kilauea Volcano, Hawaii. *Bulletin of Volcanology, 56*(5), 343-360.

Piazolo, S., Bons, P. D., Passchier, C.W., (2002), The influence of matrix rheology and vorticity on fabric development of populations of rigid objects during plane strain deformaiton, *Tectonophysics*, 351(4), 315-329.

Prior, D. J., Boyle, A. P., Brenker, F., Cheadle, M. C., Day, A., Lopez, G., Peruzzo, L., Potts, G. J., Reddy, S., & Spiess, R. (1999). The application of electron backscatter diffraction and orientation contrast imaging in the SEM to textural problems in rocks. *American Mineralogist*, *84*(11-12), 1741-1759.

Richter, F., Chaussidon, M., Mendybaev, R., & Kite, E. (2016). Reassessing the cooling rate and geologic setting of Martian meteorites MIL 03346 and NWA 817. *Geochimica et Cosmochimica Acta*, *182*, 1-23.

Shelley, D. (1985). Determining paleo-flow directions from groundmass fabrics in the Lyttelton radial dykes, New Zealand. *Journal of Volcanology and Geothermal Research*, *25*(1-2), 69-79.

Skemer, P., Katayama, I., Jiang, Z., & Karato, S.-i. (2005). The misorientation index: Development of a new method for calculating the strength of lattice-preferred orientation. *Tectonophysics*, *411*(1-4), 157-167.

Tikoff, B., & Fossen, H. (1999). Three-dimensional reference deformations and strain facies. *Journal of Structural Geology*, *21*(11), 1497-1512.

Treiman, A. H. (2005). The nakhlite meteorites: Augite-rich igneous rocks from Mars. *Chemie der Erde-Geochemistry*, *65*(3), 203-270.

Udry, A., & Day, J. M. D. (2018). 1.34 billion-year-old magmatism on Mars evaluated from the co-genetic nakhlite and chassignite meteorites. *Geochimica et Cosmochimica Acta*, *238*, 292-315.

Ventura, G., De Rosa, R., Colletta, E., & Mazzuoli, R. (1996). Deformation patterns in a high-viscosity lava flow inferred from the crystal preferred orientation and imbrication structures: an example from Salina (Aeolian Islands, southern Tyrrhenian Sea, Italy). *Bulletin of Volcanology*, *57*(7), 555-562.

Vollmer, F. W. (1990). An application of eigenvalue methods to structural domain analysis. *Geological Society of America Bulletin*, *102*(6), 786-791.

Wada, Y. (1992). Magma flow directions inferred from preferred orientations of phenocryst in a composite feeder dike, Miyake-Jima, Japan. *Journal of Volcanology and Geothermal Research*, *49*(1-2), 119-126.

Watt, L. E., Bland, P. A., Prior, D. J., & Russell, S. S. (2006). Fabric analysis of Allende matrix using EBSD. *Meteoritics & Planetary Science*, *41*(7), 989-1001.

Supplementary materials

MATLAB MTEX codeline*

Set up

startup_mtex

Import ebsd data

Run and save

Copy crystallographic information from EBSD window.

cs_aug=crystalSymmetry('12/m1', [9.7381 8.8822 5.2821], [90,106.23,90]*degree, 'X||a*',

'Y||b*', 'Z||c', 'mineral', 'Augite')

J-Index

odf_aug=calcODF(ebsd('Augite').orientations)

J_aug=textureindex(odf_aug)

M-Index

[density_uniform,~]=calcAngleDistribution(cs_aug)

density_uniform=density_uniform/sum(density_uniform)

mdf=calcMDF(odf_aug)

[density_MDF,~]=calcAngleDistribution(mdf,'resolution',1*degree)

density_MDF=density_MDF/sum(density_MDF)

M_index=(sum((abs(density_MDF-density_uniform))/2))

PGR data

o=(ebsd('Augite').orientations)

v=o*Miller(1,0,0,cs_aug,'Augite','uvw') change miller to correct crystal axis

[x,y,z]=double(v)

OT=1./numel(x)*[x,y,z]'*[x,y,z]

[Vec,Diagonal]=eig(OT)

```
value=diag(Diagonal)
[value,index]=sort(value,'descend')
vec1(1:3)=Vec(:,index(1))
vec2(1:3)=Vec(:,index(2))
vec3(1:3)=Vec(:,index(3))
NORM=value(1)+value(2)+value(3)
P100=(value(1)-value(2))/NORM
G100=(2.0*(value(2)-value(3)))/NORM
R100=(3.0*value(3))/NORM
PGR=P100+G100+R100
```

*note this codeline works for Augite. To adapt the code for another mineral phase replace crystal data, the word Augite and associated abbreviations with the mineral of interest.